

## CHAPTER 3: A MISMATCH-SELECTIVE, BIFUNCTIONAL RHODIUM-OREGON GREEN CONJUGATE: A FLUORESCENT PROBE FOR MISMATCHED DNA<sup>§</sup>

### 3.1: INTRODUCTION

Mismatch repair deficiency on the cellular level can have dire consequences on the physiological level: the accumulation of genomic mismatches and their consequent mutations create a high likelihood for cancerous transformations.<sup>1-3</sup> Indeed, mutations in MMR genes have been identified in 80% of hereditary non-polyposis colon cancers (also known as Lynch syndrome), and 15–20% of biopsied solid tumors have shown evidence of somatic mutations associated with MMR genes.<sup>4-10</sup> Moreover, MMR deficiency has also been linked to resistance to common chemotherapeutic and antineoplastic agents such as doxorubicin and cisplatin.<sup>9, 11, 12</sup>

Given these profound links between mismatch repair deficiency and cancer, the development of our unique recognition technology for diagnostic applications has been an important focus of our laboratory.<sup>13-16</sup> Indeed, one can envision two types of metalloinsertor-based diagnostics for mismatch repair deficiency: (1) an *in vitro* probe that could be employed to interrogate the extracted DNA of biopsied cancer cells and (2) an *in vivo* agent that could be used to investigate intact DNA within cultured tumor cells.

In both scenarios, fluorescence is a particularly attractive reporter.<sup>17-20</sup> Consequently, we have previously used a ruthenium-based probe designed to

---

<sup>§</sup> Adapted from Zeglis, B. M.; Barton, J. K. A mismatch-selective bifunctional rhodium-Oregon Green conjugate: A fluorescent probe for mismatched DNA. *J. Am. Chem. Soc.* **2006**, *128*, 5654–5655.

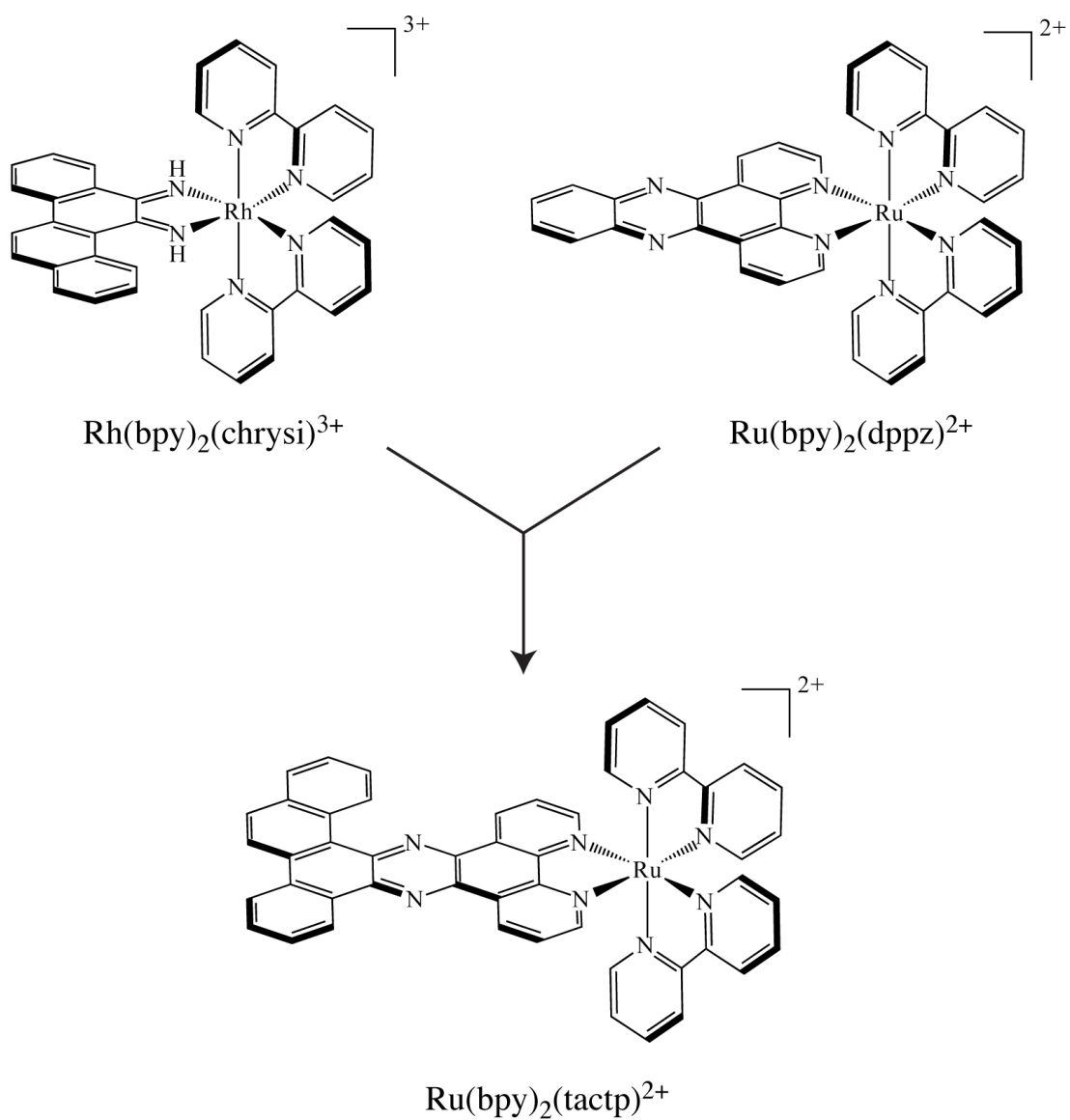


**Figure 3.1: Design of  $\text{Ru}(\text{bpy})_2(\text{tactp})^{2+}$ .** The ruthenium bisdipyridyl complex bears a sterically expansive, luminescent ligand that is a structural chimera of the chrysi and dppz ligands.

fluoresce specifically in the presence of mismatched DNA (**Figure 3.1**).<sup>21</sup> The metal complex,  $\text{Ru}(\text{bpy})_2(\text{tactp})^{2+}$ , seeks to combine in a single entity the DNA light-switch character of the  $\text{Ru}(\text{dppz})(\text{L})_2^{2+}$  family of complexes and the mismatch-specificity of the  $\text{Rh}(\text{chrysi})(\text{L})_2^{3+}$  class of agents. To this end, a chimeric ligand, tactp (4,5,9,18-tetraazachryseno[9,10-b]-triphenylene), that contains the critical structural features of both chrysene-5,6-quinone (chrysi) and dipyrido[3,2-*a*:2',3'-*c*]phenazine (dppz) was synthesized and metallated onto a ruthenium bisdipyridyl platform. Singlet oxygen sensitization experiments confirm that the complex does, indeed, selectively bind mismatched sites in duplex DNA; however, the avid dimerization of the expansive aromatic ligand leads to high levels of non-specific fluorescence and thus dramatically limits its diagnostic potential.

The significant limitations of the single metal complex  $\text{Ru}(\text{bpy})_2(\text{tactp})^{2+}$  system led us to pursue a markedly different avenue: bifunctional conjugates. Anatomically, bifunctional conjugates are tripartite, composed of metalloinsertor, linker, and payload subunits.<sup>22-24</sup> In this case, the mismatch-specific metalloinsertor would be covalently tethered to an organic fluorophore, thus conferring mismatch-specificity on the otherwise non-specific fluorescent moiety (**Figure 3.2**). Of course, simply getting the fluorophore in the proximity of mismatched DNA is not good enough. Ideally, a mismatch-specific fluorophore would be inactivated when in free solution or in the presence of matched DNA and selectively activated in the presence of mismatched DNA. Separating the metalloinsertor and fluorophore subunits in a bifunctional conjugate eliminates the possibility of the useful light-switch behavior characteristic of the  $\text{Ru}(\text{dppz})\text{L}_2^{2+}$  complexes. However, the two component, bifunctional system lends itself

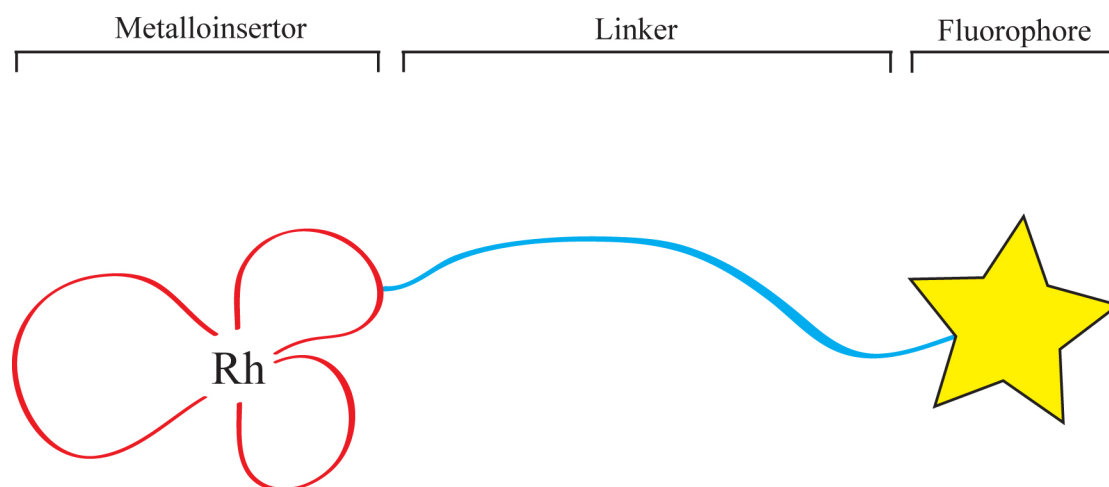


**Figure 3.2: The anatomy of a bifunctional conjugate.** In the case of a mismatch-specific fluorophore, a metalloinsertor subunit (red) is covalently linked (blue) to an organic fluorophore (yellow).

extremely well to an alternative strategy for achieving fluorescence selectivity: differential intramolecular quenching.

The strategy is quite simple: a flexible linker will covalently attach a positively charged, mismatch-specific metalloinsertor and a negatively charged, organic fluorophore. In the absence of DNA, the positively-charged rhodium complex will ion pair with the negatively charged fluorophore, thus quenching its fluorescence (**Figure 3.3**). The same will be true in the presence of matched DNA, for the mismatch-selective metalloinsertor will not interact with the well-matched oligonucleotide. In the presence of mismatched DNA, in contrast, the metalloinsertor will selectively bind the mismatched sites, and the negatively charged phosphodiester backbone will repel the fluorophore away from the DNA and the rhodium moiety, reducing quenching and increasing fluorescence.

Herein, we report the design, synthesis, and fluorescence testing of bifunctional conjugates for the selective detection of mismatched DNA.

## **3.2: RESULTS AND DISCUSSION**

### **3.2.1: FIRST GENERATION CONJUGATE**

#### **3.2.1.1: SYNTHESIS AND CHARACTERIZATION**

The first generation conjugate was assembled sequentially from  $\text{RhCl}_3$ . In order to facilitate conjugation, a trisheteroleptic metalloinsertor,  $\text{Rh}(\text{phen})(\text{chrysi})(^{\text{NH}_2}\text{bpy})^{3+}$ , was first synthesized according to published protocols (**Figure 3.4**). A dimethyl-bipyridine ligand bearing an aliphatic aminohexyl chain,  $^{\text{NH}_2}\text{bpy}$ , was employed to provide the flexible linker between the metalloinsertor and fluorophore.

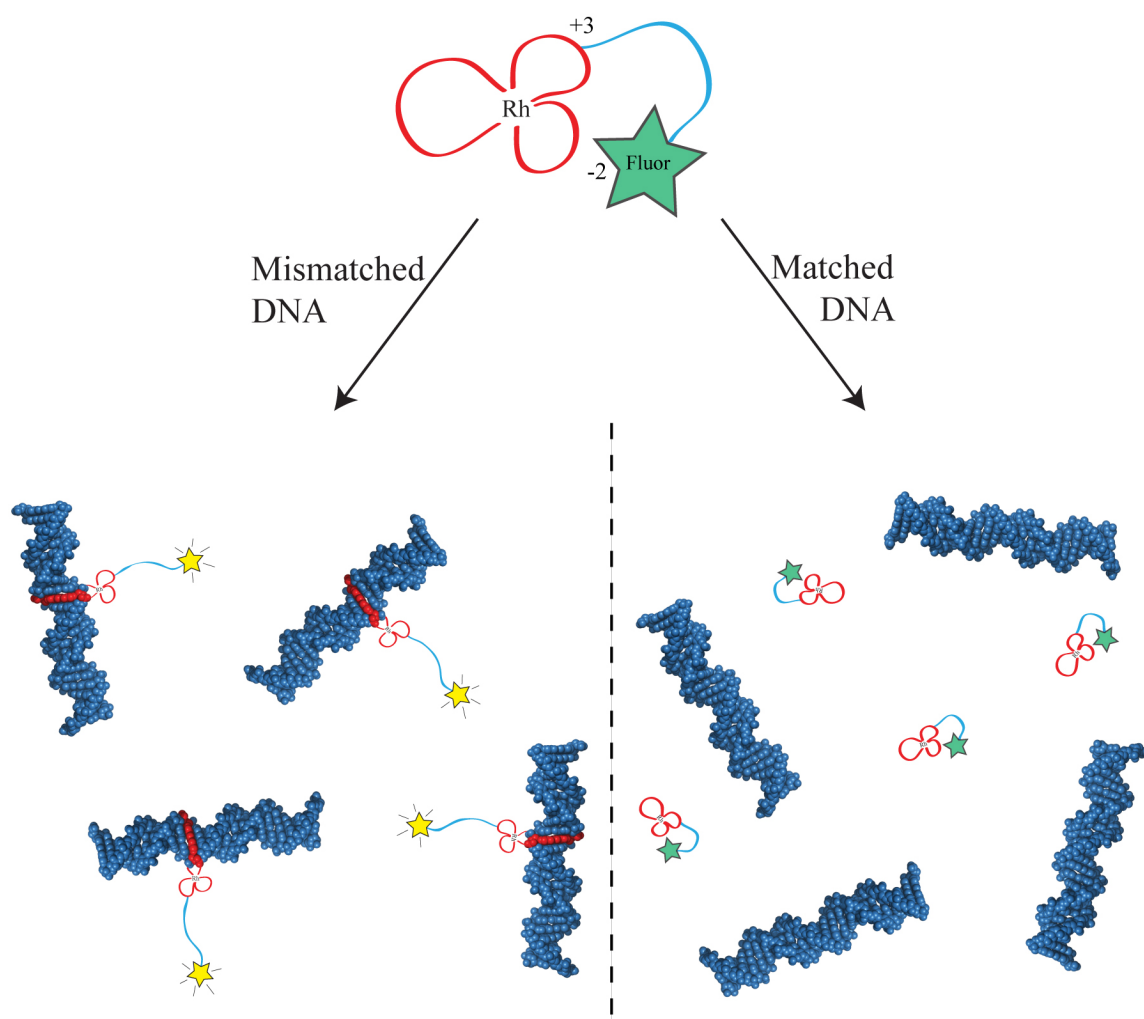


**Figure 3.3: Differential intramolecular quenching scheme.** In the absence of DNA or presence of matched DNA, the rhodium and fluorophore moieties will ion pair, dramatically quenching the fluorescence of the latter. In the presence of mismatched DNA, the metalloinsertor will bind the oligonucleotide, and the negatively charged phosphate backbone will repel the fluorophore away from the rhodium and the DNA, reducing quenching and increasing fluorescence.

Oregon Green 514<sup>TM</sup> (Molecular Probes, Invitrogen) was chosen for the fluorophore for three reasons: it is water soluble, it is negatively charged (-2 at pH 7), and it does not interact with DNA. The trisheteroleptic metalloinsertor moiety was easily coupled to the commercially-available succinimidyl ester of Oregon Green 514<sup>TM</sup> in DMF at room temperature (**Figure 3.5**). The completed conjugate was purified via cation exchange chromatography and reverse-phase HPLC using an HP1100 HPLC system, a Varian DynaMax C18 semipreparative column, and an elution gradient of 85:15 to 40:60 H<sub>2</sub>O (0.1% TFA):MeCN (0.1% TFA) over 60 min.

The first generation metalloinsertor-Oregon Green conjugate (RhOG) was characterized via UV-Vis and fluorescence spectroscopy. Not surprisingly, the absorbance spectrum of the conjugate resembles the sum of the spectra of the two subunits, with metalloinsertor bands at 303 nm and 313 nm and a large fluorophore peak at 519 nm (**Figure 3.6a**). Fluorescence studies of RhOG reveal excitation and emission maxima at 519 and 530 nm, respectively, slightly shifted relative to the parent Oregon Green fluorophore (**Figure 3.7b**). As expected, the fluorescence of RhOG is dramatically quenched relative to both free Oregon Green and an equimolar, 1:1 solution of Rh(phen)(chrysi)(<sup>NH<sub>2</sub></sup>bpy)<sup>3+</sup> and Oregon Green. Further, fluorescence titrations of untethered Oregon Green and untethered Rh(phen)(chrysi)(<sup>NH<sub>2</sub></sup>bpy)<sup>3+</sup> eliminate the inner filter effect and an energy transfer quenching mechanism and instead support electron transfer as the source of quenching.

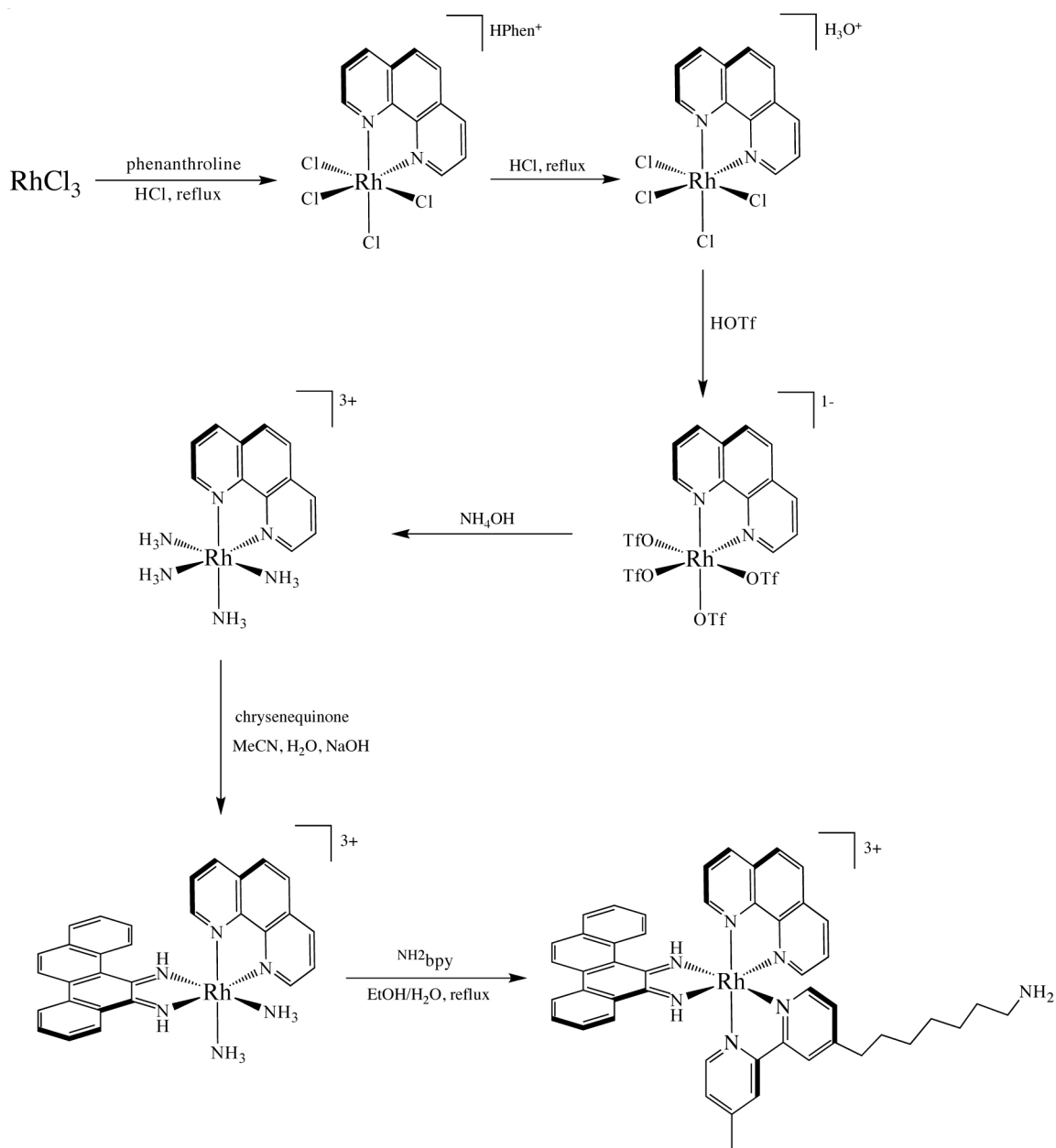


**Figure 3.4. Synthesis of the trisheteroleptic metalloinsertor subunit.** The conjugate's metalloinsertor subunit was synthesized via the sequential addition of phen, chrysi, and  $\text{NH}_2\text{bpy}$  ligands onto a rhodium center.

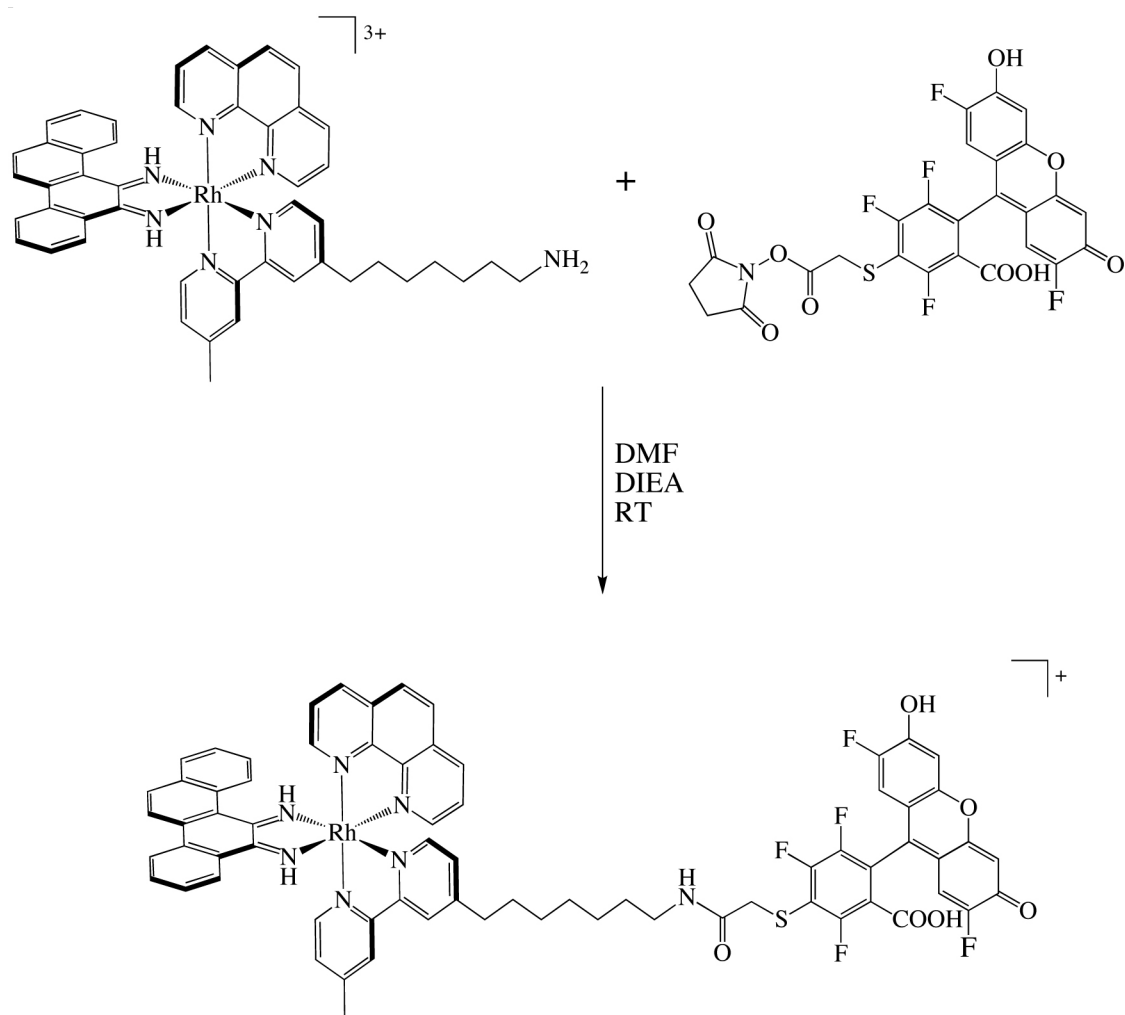
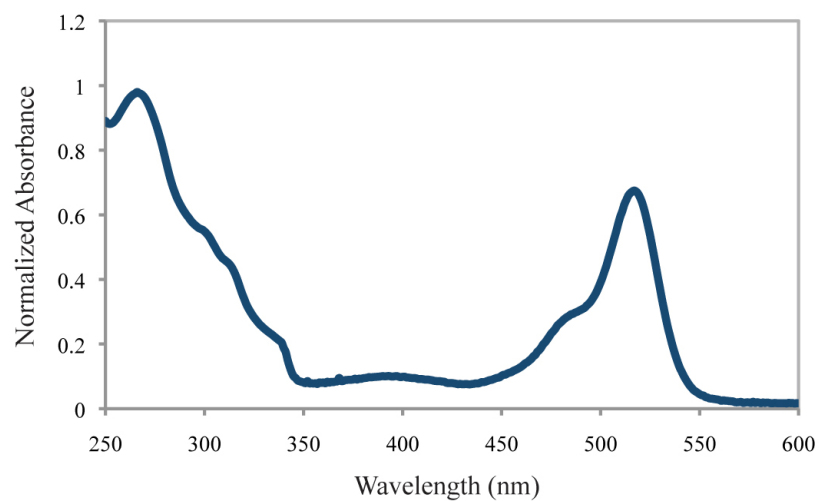


**Figure 3.5: Synthesis of RhOG.** The metalloinsertor-Oregon Green conjugate was synthesized via the facile coupling of the pendant amine of the rhodium complex to the succinimidyl ester of the commercially available fluorophore starting material.

A.



B.

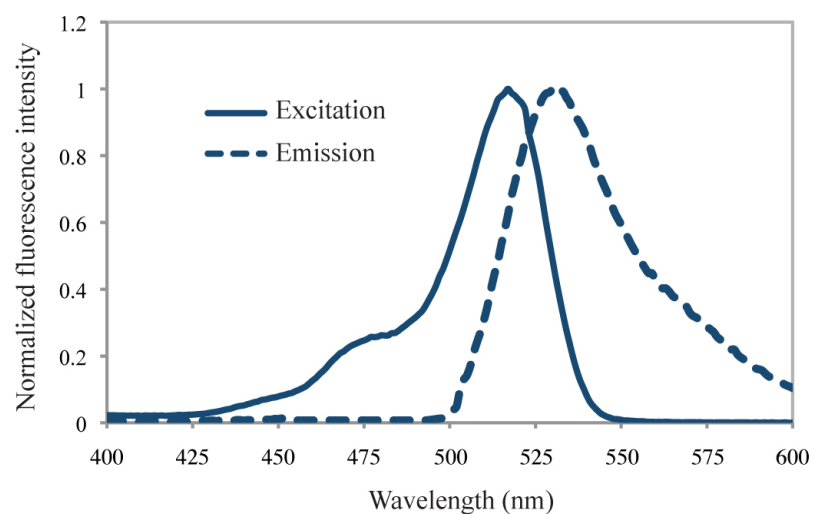


**Figure 3.6: Absorbance and fluorescence spectra of RhOG.** (A) The UV-Vis spectrum of RhOG:  $\lambda_{\text{max}}$  303 nm ( $\epsilon = 54,800$ ), 313 ( $\epsilon = 44,600$ ), 519 ( $\epsilon = 78,000$ ). (B) The fluorescence excitation (solid line) and emission (dotted line) spectra of RhOG, showing  $\lambda_{\text{ex}} = 519$  nm and  $\lambda_{\text{em}} = 530$  nm.

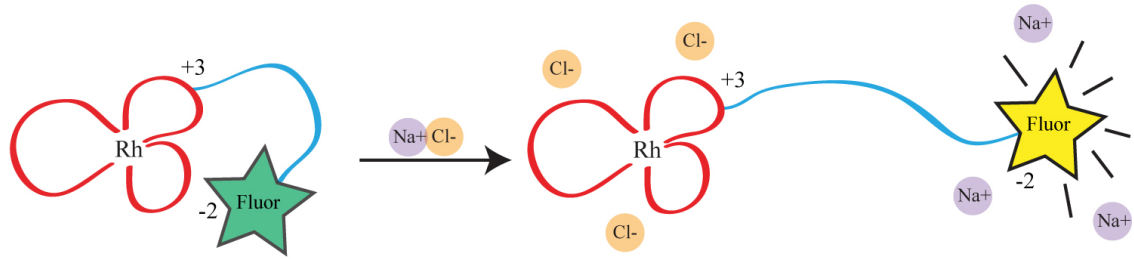
In order to investigate the intramolecular quenching behavior of RhOG, fluorescence measurements of 1  $\mu\text{M}$  conjugate in the presence of variable salt concentrations (10 mM NaPi, 0–500 mM NaCl, pH 7.1) were taken. A mild dependence of fluorescence on ion strength was revealed. The emission of RhOG, while still significantly quenched relative to Oregon Green, increases almost 5-fold over the range of NaCl concentrations tested. Neither Oregon Green alone nor an untethered 1:1 solution of Rh(phen)(chrysi)(<sup>NH<sub>2</sub></sup>bpy)<sup>3+</sup> and Oregon Green shows variation in fluorescence with ionic strength. These observations support an intramolecular ion-pair mechanism of quenching; as the salt concentration increases, the Rh•OG ion pair can separate more easily, attenuating quenching and increasing fluorescence (**Figure 3.7**).

### 3.2.1.2: PHOTOCLEAVAGE EXPERIMENTS

For DNA experiments, two 17-mer oligonucleotides were synthesized and purified, each either containing or lacking a central C•C mispair: 5'-CAC ATG CAC GAC GGC GC-3' (in the well-matched oligonucleotide, a guanine is complementary to the bold cytosine; in the mismatched oligonucleotide, a cytosine is complementary at the site).

Mismatch targeting by the bifunctional conjugate was first examined via PAGE experiments using 5'-<sup>32</sup>P-labeled oligonucleotides. First, a simple photocleavage experiment was employed to determine whether RhOG and its trisheteroleptic metalloinsertor subunit did, indeed, recognize and photocleavage mismatched DNA. In this experiment, matched or mismatched duplex DNA (1  $\mu\text{M}$ ) was incubated with 1  $\mu\text{M}$

A.



B.

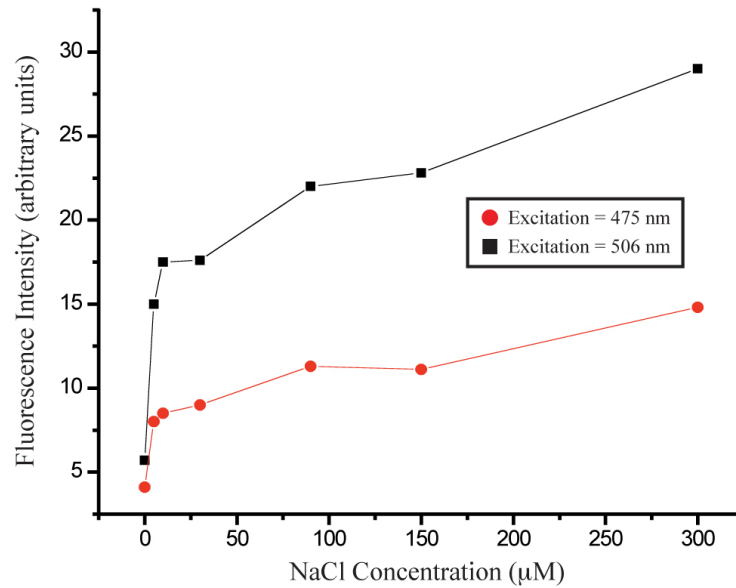


**Figure 3.7: Dependence of ionic strength on the fluorescence of RhOG.** (A)

Schematic showing the hypothesized role of salt in the ion-pairing of RhOG; (B) plot of the fluorescence of RhOG at 530 nm as a function of ionic strength (500 nM RhOG, 10 mM NaPi, pH 7.1)

RhOG and Rh(phen)(chrysi)(<sup>NH<sub>2</sub></sup>bpy)<sup>3+</sup> and irradiated for 5 min on an Oriel Instruments solar simulator (**Figure 3.8**).

Autoradiography of the gel clearly reveals that both RhOG and Rh(phen)(chrysi)(<sup>NH<sub>2</sub></sup>bpy)<sup>3+</sup> specifically recognize and cleave mismatched sites in DNA. No photocleavage nor any other evidence for matched site binding is evident. Significantly, it appears that RhOG is a weaker binder than its rhodium subunit alone, likely a consequence of the former's reduced charge.

A photocleavage titration was next used to determine the site-specific binding constant of the conjugate. In this experiment, radiolabeled, mismatched DNA (1 μM) was incubated with variable concentrations of RhOG (100 nM to 10 μM) and irradiated for 10 min on a solar simulator. Autoradiography of the resultant gel and subsequent quantification using ImageQuant software indicate a site-specific binding constant of  $4 \times 10^5 \text{ M}^{-1}$ . This value is consistent with measurements for the parent Rh(bpy)<sub>2</sub>(chrysi)<sup>3+</sup> complex and for other bifunctional conjugates; the affinity of RhOG, however, is slightly reduced compared to previous cases, again possibly a consequence of its reduced charge.<sup>13, 22, 23, 25</sup>

### 3.2.1.3: FLUORESCENCE MEASUREMENTS

Armed with an understanding of the site-specificity of the conjugate, we next embarked upon fluorescence titrations with matched and mismatched DNA. In these experiments, 1 μM RhOG was added to variable amounts of the matched and mismatched oligonucleotides described above. In all experiments, a wavelength of 475

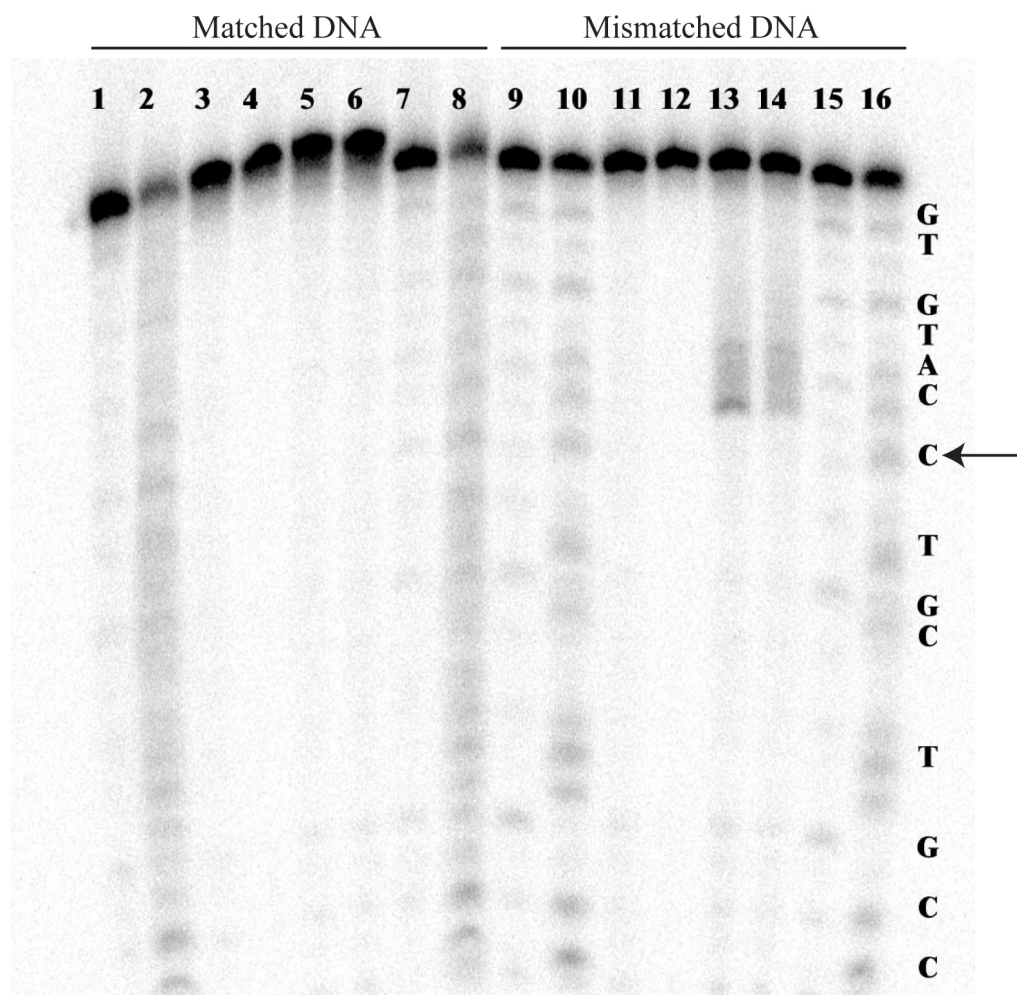


**Figure 3.8: RhOG photocleavage gel.** Autoradiogram of a denaturing 20% polyacrylamide gel revealing DNA photocleavage for RhOG and its rhodium subunit. Conditions are duplex (1  $\mu$ M), Rh (1  $\mu$ M) in 20 mM NaCl, 10 mM NaPi, in pH 7.1 followed by irradiation for 5 min with a solar simulator. Lanes 1, 2, 7, 8, 9, 10, 15, and 16 show Maxam Gilbert sequence reactions for matched (1, 2, 7, 8) and mismatched (9, 10, 15, 16) DNA. For matched and mismatched DNA, respectively: lanes 3 and 11 show light controls (irradiation, no RhOG); lanes 4 and 12 show dark controls (RhOG with no irradiation); lanes 5, 6, 13, and 14 show DNA after irradiation in the presence of Rh(phen)(chrysi)( $\text{NH}_2\text{bpy}$ ) $^{3+}$  (5, 13) and RhOG (6, 14). The DNA sequence is 5'- $^{32}\text{P}$ -GCGCCGTCGTXCATGTG-3' where X = C or G. The complement contains a matched or mismatched C complementary to the bold X site. The arrow marks the mismatched site.

nm was employed for excitation (to avoid emission interference from scattered light), and the emission was monitored at 530 nm.

Despite the known binding selectivity of the conjugate, only a slight increase in fluorescence is observed with mismatched DNA when compared to matched DNA; at saturating DNA concentrations, the relative intensity with mismatched versus matched DNA is  $1.3 \pm 0.1$  (**Figure 3.9**). Significantly, the fluorescence of the conjugate remains very quenched in the presence of both types of oligonucleotide. Further, in control experiments, no mismatch-dependent differences in fluorescence are found for Oregon Green alone or for a 1:1 solution of  $\text{Rh}(\text{phen})(\text{chrysi})(^{\text{NH}_2}\text{bpy})^{3+}$  and Oregon Green. Further still, RhOG shows no increased fluorescence with single stranded DNA. Taken together, these data indicate that the bifunctional conjugate does, indeed, display enhanced fluorescence with mismatched DNA. Granted, the differential is slight; however, the success, though limited, paved the way for the optimization of the system.

### **3.2.2: SECOND GENERATION CONJUGATES**

#### **3.2.2.1: SYNTHESIS AND CHARACTERIZATION**

The limited success of RhOG prompted a reevaluation of the conjugate's design. The ionic strength dependence and DNA titration data clearly indicate that RhOG is capable of the intramolecular quenching mechanism envisioned for the system. However, the ultimately meager differential fluorescence displayed by the conjugate suggests that while an "closed" to "open" (quenched to unquenched) conformational shift is possible in the presence of salt or mismatched DNA, the "open" configuration simply remains too quenched for the molecule to display any dramatically differential fluorescence. It was

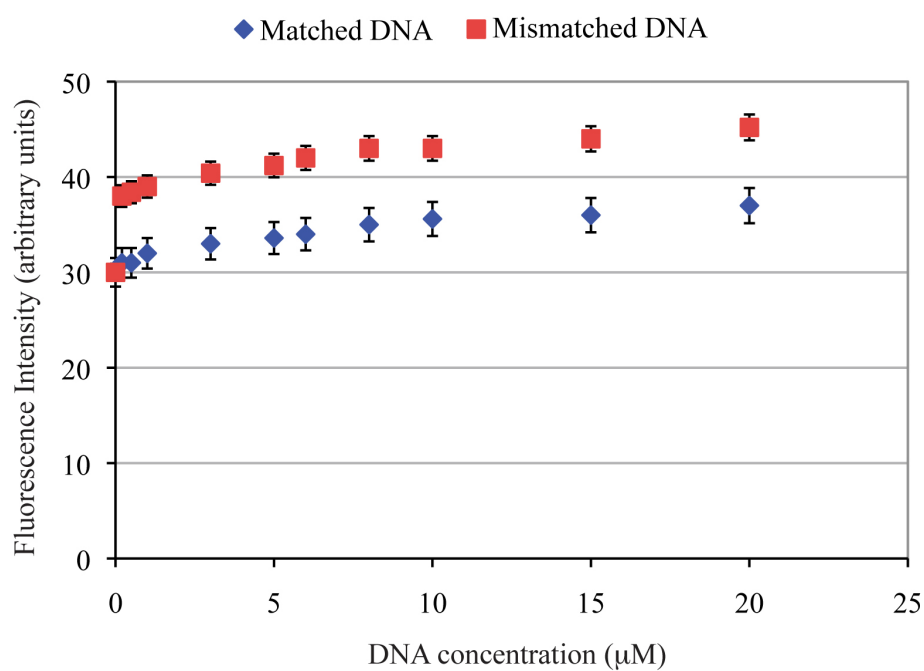


**Figure 3.9: Fluorescence of RhOG with matched and mismatched DNA.** The DNA titration shows a slight (25%) increase in the fluorescence of the conjugate in the presence of mismatched DNA when compared to matched DNA. Conditions: 1 μM RhOG, 20 mM NaCl, 10 mM NaPi, pH 7.1

hypothesized that this behavior arises simply because the metalloinsertor quencher and fluorophore are too close together. Put simply, the conjugate remains too quenched in the “open” state.

To counter this problem, three new conjugates with elongated linkers were designed and synthesized. Of course, the first step in this process was the synthesis of the three novel linker-modified bipyridine ligands. The first, nicknamed <sup>el</sup>bpy, bears a 11 carbon aliphatic linker similar to that in the aforementioned <sup>NH<sub>2</sub></sup>bpy. Not surprisingly, <sup>el</sup>bpy was synthesized in a similar manner. 4,4'-dimethylbipyridine is first monoalkylated with LDA and 1,10-dibromodecane. Then, the bromide-terminated chain of the alkylation product was converted to an amine-terminated linker through a phthalimide intermediate via the Gabriel synthesis (**Figure 3.10**, see EXPERIMENTAL).

During the synthesis of <sup>el</sup>bpy, it became evident that any aliphatic linker longer than ten carbons would present serious solubility problems. Therefore, two additional new ligands were synthesized to contain an ethylene glycol (more rigorously, dioxethane) unit within the linker. The first, <sup>peg</sup>bpy, contains a 14 atom linker and can be synthesized in five steps from 4,4'-dimethylbipyridine by analogy to the methods of Della Ciana *et al.*<sup>28</sup> First, the starting material is monoalkylated with LDA and 2-(3-bromopropyl)-1,3-dioxolane. The dioxolane is then deprotected under acidic conditions to yield the corresponding aldehyde, which is then oxidized with potassium permanganate to a carboxylic acid. This carboxylic acid is converted to a succinimidyl ester with N-hydroxysuccinimide and DCC. Finally, the NHS ester is coupled to 2,2'-(ethylenedioxy)bis(ethylamine) to yield the final <sup>peg</sup>bpy product (**Figure 3.11**).

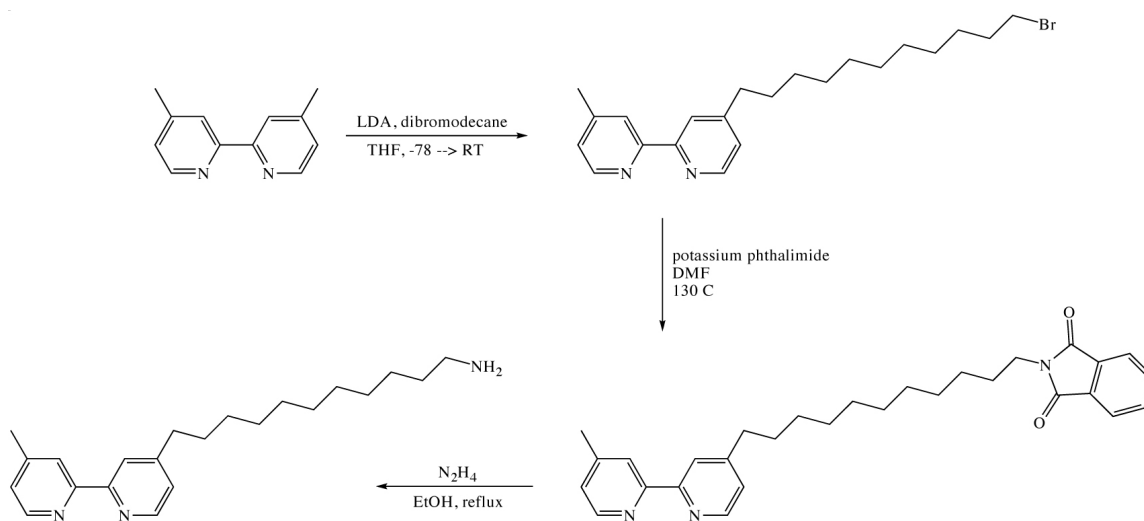


**Figure 3.10: Synthesis of  $^{el}bpy$ .** The modified bipyridine with an amine-terminated, eleven carbon aliphatic linker was synthesized in three steps from 4,4'-dimethylbipyridine via the Gabriel amine synthesis.<sup>26, 27</sup>

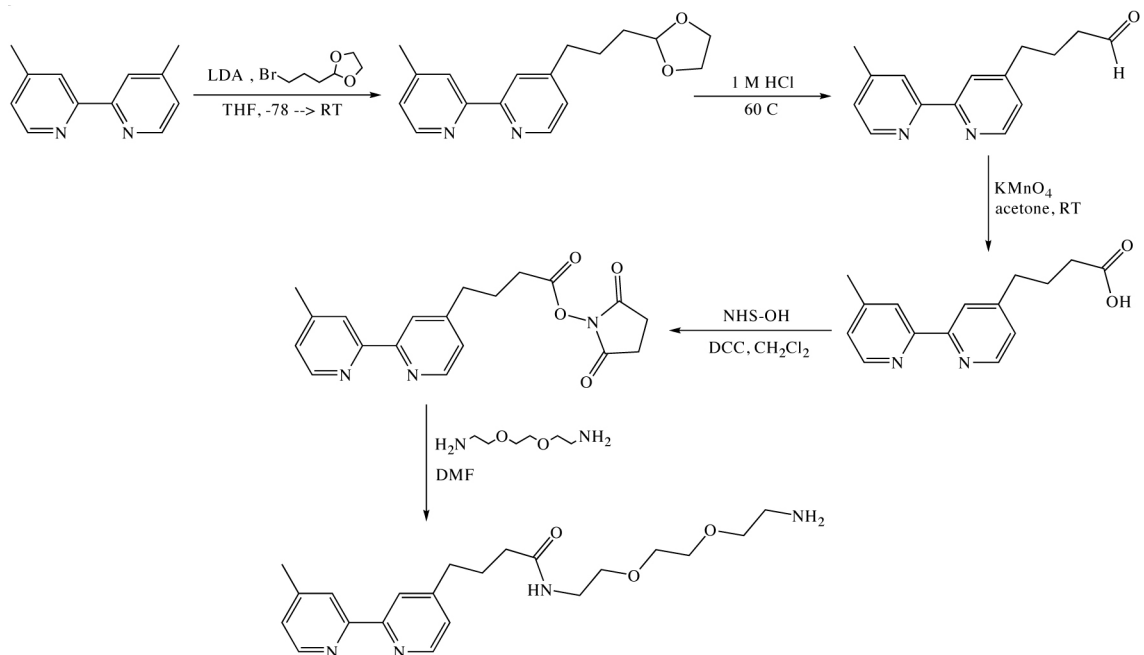
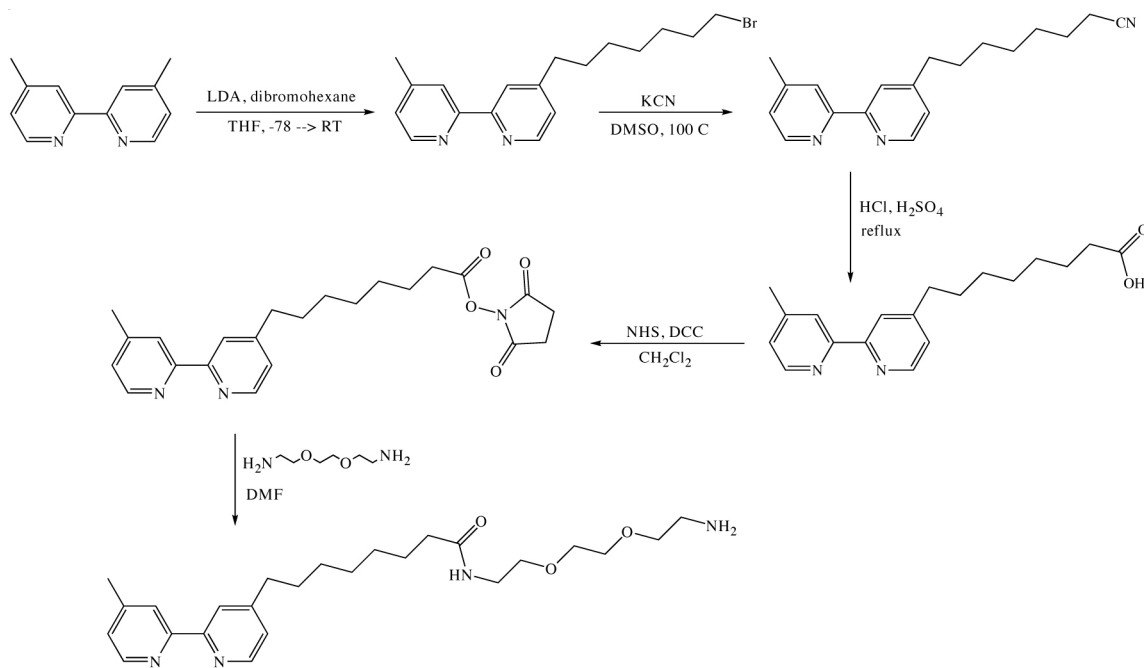


**Figure 3.11: Synthesis of <sup>peg</sup>bpy.** The ligand bears an 14 atom linker and is synthesized in five steps from 4,4'-dimethylbipyridine via sequential alkylation, deprotection, oxidation, and coupling reactions.

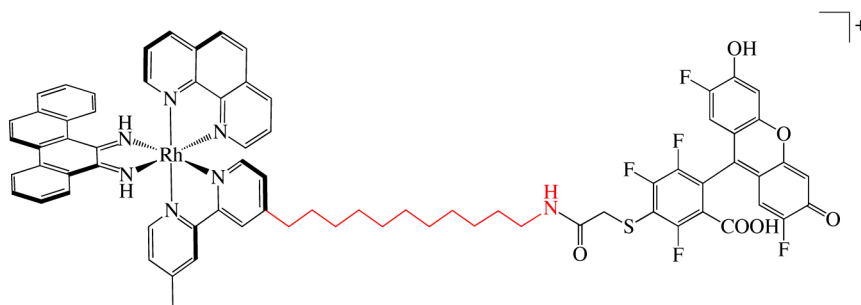
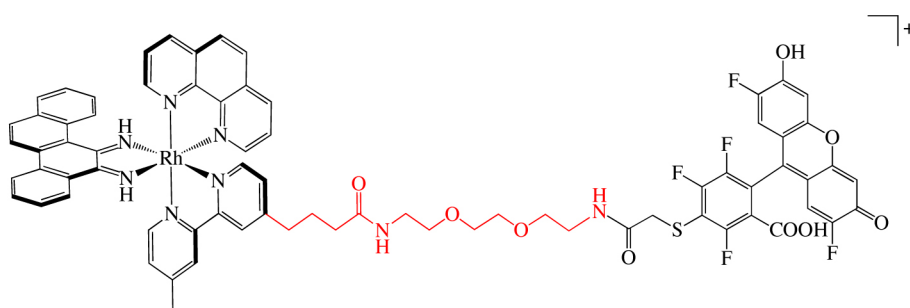
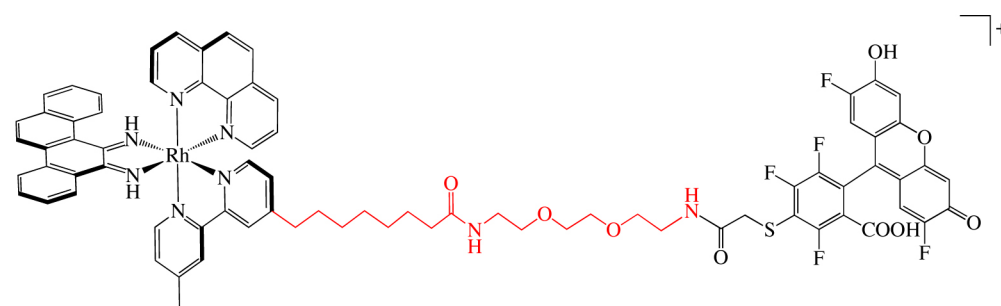
The third ligand, <sup>lpeg</sup>bpy, contains a 17 atom linker and was also synthesized in five steps from 4,4'-dimethylbipyridine, though by a different strategy. First, the aliphatic linker was installed onto 4,4'-dimethylbipyridine via monoalkylation with LDA and dibromohexane. The bromide group terminating the linker was then converted to a carboxylic in two steps through a cyanide intermediate. Finally, this carboxylic acid was converted to the final <sup>lpeg</sup>bpy ligand through a succinimidyl ester intermediate (**Figure 3.12**).

With the linker-modified ligands complete, the trisheteroleptic metalloinsertor subunits were assembled sequentially from RhCl<sub>3</sub> as described above. As with RhOG, each metalloinsertor was then coupled to the succinimidyl ester of Oregon Green 514 to yield three new bifunctional conjugates: <sup>el</sup>RhOG, <sup>peg</sup>RhOG, and <sup>lpeg</sup>RhOG (**Figure 3.13**). All three conjugates were purified via reverse phase HPLC (see EXPERIMENTAL).

The three new conjugates — <sup>el</sup>RhOG, <sup>peg</sup>RhOG, and <sup>lpeg</sup>RhOG — were characterized via UV-Vis and fluorescence spectroscopy. As with RhOG, the absorbance spectrum of each conjugate resembles the additive combination of the spectra of the two subunits, with metalloinsertor bands at 303 nm and 313 nm and a large fluorophore peak at 519 nm (**Figure 3.14**). Not surprisingly, fluorescence studies of the second generation conjugates revealed more similarities to the first generation version. Each conjugate is characterized by excitation and emission maxima at 519 and 530 nm, respectively, again red-shifted relative to the parent Oregon Green fluorophore (**Figure 3.15**). Further, like RhOG, the fluorescence of each conjugate is significantly quenched relative to both free Oregon Green and an equimolar, 1:1 solution of Oregon Green and either Rh(phen)(chrysi)(<sup>el</sup>bpy)<sup>3+</sup>, Rh(phen)(chrysi)(<sup>peg</sup>bpy)<sup>3+</sup>, Rh(phen)(chrysi)(<sup>lpeg</sup>bpy)<sup>3+</sup>.



**Figure 3.12: Synthesis of <sup>lpeg</sup>bpy.** The ligand is synthesized in five steps from 4,4'-dimethylbipyridine via monoalkylation, cyanide substitution, hydrolysis, and coupling steps.

$^{\text{el}}\text{RhOG}$ : $^{\text{peg}}\text{RhOG}$ : $^{\text{lpeg}}\text{RhOG}$ :

**Figure 3.13: Structures of  $^{\text{el}}\text{RhOG}$ ,  $^{\text{peg}}\text{RhOG}$ , and  $^{\text{lpeg}}\text{RhOG}$ .** The new, elongated linkers are displayed in red.

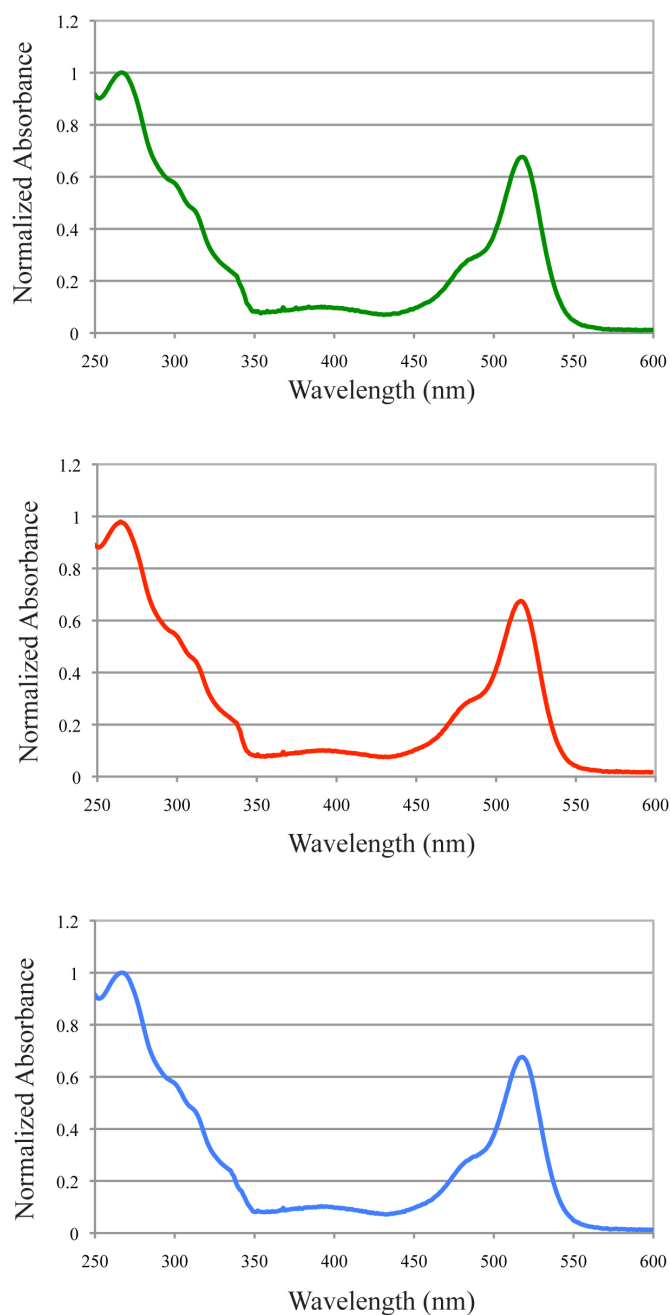


**Figure 3.14: The UV-Vis spectra of the second generation <sup>x</sup>RhOG conjugates.** The absorption spectra of <sup>el</sup>RhOG (green), <sup>peg</sup>RhOG (red), and <sup>lpeg</sup>RhOG (blue) are shown. The extinction coefficients for the conjugates in question are identical:  $\lambda_{\text{max}}$  303 nm ( $\epsilon = 54,800$ ), 313 ( $\epsilon = 44,600$ ), and 519 ( $\epsilon = 78,000$ ).

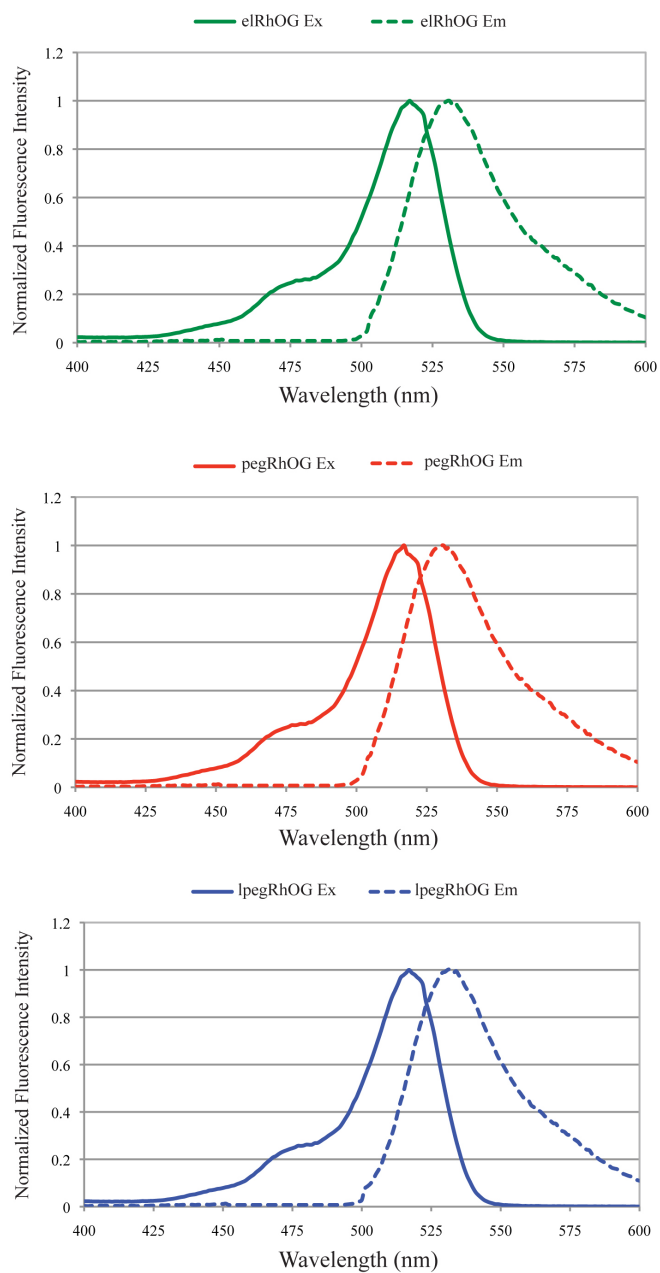


**Figure 3.15: The fluorescence spectra of the second generation <sup>x</sup>RhOG conjugates.** The excitation (solid line) and emission (dotted line) fluorescence spectra of <sup>el</sup>RhOG (green), <sup>peg</sup>RhOG (red), and <sup>lpeg</sup>RhOG (blue) are shown. The three spectra are virtually identical, with excitation maxima of 519 nm and emission maxima of 530 nm.

For example, for <sup>peg</sup>RhOG, the ratio of the fluorescence intensity of conjugate : equimolar untethered subunits : free Oregon Green is 1 : 73 : 100.

Fluorescence measurements were taken at variable ionic strengths in order to investigate the intramolecular quenching behavior of the new conjugates. For each conjugate, emission measurements (excitation = 475 nm, emission = 530 nm) of 1  $\mu$ M <sup>x</sup>RhOG in the presence of variable concentrations of salt (10 mM NaPi, 0–500 mM NaCl, pH 7.1) were taken. For <sup>peg</sup>RhOG and <sup>lpeg</sup>RhOG, a strong dependence of fluorescence on ionic strength is observed. In both cases, the fluorescence emission of the conjugate increases over 15-fold as the sodium chloride concentration is increased from 0 to 500 mM. These data strongly support an intramolecular ion-pair mechanism of quenching for these conjugates. Perhaps more importantly, these values reveal that the longer, more flexible linkers of <sup>peg</sup>RhOG and <sup>lpeg</sup>RhOG confer a greater dynamic range of fluorescence intensities on these conjugates compared to the first generation RhOG molecule. Put more simply, these linkers allow the rhodium and fluorophore subunits to separate more fully in the “open” state, attenuating quenching even further and leading to a larger fluorescence increase.

<sup>el</sup>RhOG, in contrast, exhibits far different behavior. The fluorescence of this conjugate displays no dependence on the ionic strength of the solution. It thus becomes apparent that this conjugate cannot perform the conformational shift necessary for intramolecular quenching, likely a consequence of the hydrophobicity of the eleven carbon aliphatic linker. It is possible that the alkyl chain contracts on itself in aqueous solution to avoid interaction with water, thus preventing the “open” vs. “closed” transition necessary for differential and ionic strength-responsive quenching.

### 3.2.2.2: PHOTOCLEAVAGE EXPERIMENTS

For DNA experiments, two 17-mer oligonucleotides were employed, each either containing or lacking a central C•C mispair: 5'-CAC ATG CAC GAC GGC GC-3' (in the well-matched oligonucleotide, a guanine is complementary to the bold cytosine; in the mismatched oligonucleotide, a cytosine is complementary at the site). As with RhOG, mismatch targeting was first examined via PAGE experiments. Initially, simple photocleavage experiments were employed to determine whether  $^{el}$ RhOG,  $^{peg}$ RhOG, and  $^{lpeg}$ RhOG were capable of the selective recognition and photoactivated scission of mismatched DNA. In the experiment, matched and mismatched duplex DNA (1  $\mu$ M) were incubated with 1  $\mu$ M of either  $^{el}$ RhOG,  $^{peg}$ RhOG, or  $^{lpeg}$ RhOG and irradiated for 5 min on an Oriel Instruments solar simulator. Autoradiography of the resultant gel (**Figure 3.16**) reveals that all three conjugates recognize and photocleave mismatched DNA. Not surprisingly, no photocleavage at matched sites is apparent for any of the conjugates.

Subsequently, photocleavage titrations were employed to determine the specific binding constant of the conjugates to the mismatched site. In these experiments, radiolabeled, mismatched DNA (1  $\mu$ M) was incubated with variable concentrations of either  $^{el}$ RhOG,  $^{peg}$ RhOG, or  $^{lpeg}$ RhOG (100 nM to 10  $\mu$ M) and irradiated for 10 min on a solar simulator. Autoradiography of the gels and subsequent quantification using ImageQuant software revealed a site-specific binding constants of  $2 \times 10^5 \text{ M}^{-1}$  ( $^{el}$ RhOG),  $6 \times 10^5 \text{ M}^{-1}$  ( $^{peg}$ RhOG), and  $7 \times 10^5 \text{ M}^{-1}$  ( $^{lpeg}$ RhOG). These values are consistent with measurements for RhOG, Rh(bpy)<sub>2</sub>(chrysi)<sup>3+</sup>, and other bifunctional conjugates.

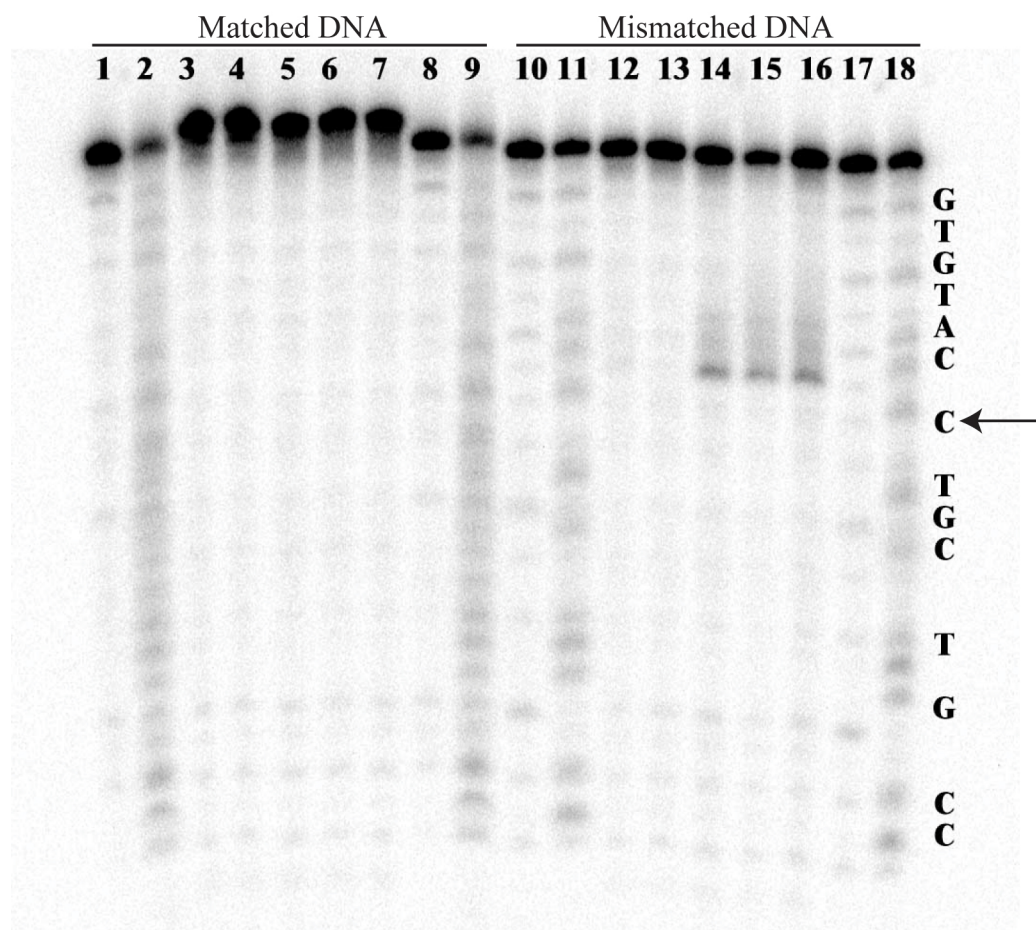


**Figure 3.16:  $^3\text{RhOG}$  photocleavage gel.** Autoradiogram of a denaturing 20% polyacrylamide gel revealing mismatch recognition and photocleavage by  $^{\text{el}}\text{RhOG}$ ,  $^{\text{peg}}\text{RhOG}$ , and  $^{\text{lpeg}}\text{RhOG}$ . Conditions are duplex (1  $\mu\text{M}$ ), Rh (1  $\mu\text{M}$ ) in 20 mM NaCl, 10 mM NaPi, in pH 7.1 followed by irradiation for 5 min with a solar simulator. Lanes 1, 2, 8, 9, 10, 11, 17, and 18 show Maxam Gilbert sequence reactions for matched (1, 2, 8, 9) and mismatched (10, 11, 17, 18) DNA. For matched and mismatched DNA, respectively: lanes 3 and 12 show light controls (irradiation, no Rh); lanes 4 and 13 show dark controls (no irradiation); lanes 5, 6, 7, 14, 15, and 16 show DNA after irradiation in the presence of  $^{\text{el}}\text{RhOG}$  (5, 14),  $^{\text{peg}}\text{RhOG}$  (6, 15), and  $^{\text{lpeg}}\text{RhOG}$  (7, 16). The DNA sequence is 5'- $^{32}\text{P}$ -GCGCCGTCGTXCATGTG-3' where X = C or G. The complement contains a matched or mismatched C complementary to the bold X site. The arrow marks the mismatched site.

Further, these affinities, like that of RhOG, are slightly reduced compared to the parent complexes, again possibly a consequence of the reduced charge of the conjugates.

### 3.2.2.3: FLUORESCENCE MEASUREMENTS

Fluorescence measurements with matched and mismatched DNA were able to provide insight into the potential of these second generation conjugates as mismatch-specific fluorophores. In these experiments, 1  $\mu\text{M}$   $^{\text{x}}\text{RhOG}$  was added to variable concentrations of the matched and mismatched oligonucleotides (described above) in buffer (20 mM NaCl, 10 mM NaPi, pH 7.1). A wavelength of 475 nm was employed for excitation (to avoid emission interference from scattered light), and the emission was monitored at 530 nm.

This line of investigation first revealed that  $^{\text{el}}\text{RhOG}$  shows very little, if any, enhanced fluorescence with mismatched DNA compared to matched DNA ( $F_{\text{mm}}/F_{\text{m}} = 1.1 \pm 0.1$ ). This is not a surprise, especially given the apparent inability of  $^{\text{el}}\text{RhOG}$  to perform the differential intramolecular quenching desired for the system.

However, over the range of DNA concentrations studied,  $^{\text{peg}}\text{RhOG}$  and  $^{\text{lpeg}}\text{RhOG}$  show *significantly* greater fluorescence with mismatched DNA than with matched DNA. Indeed, at saturating DNA concentrations, the relative fluorescence intensities of the two conjugates with mismatched versus matched DNA are  $3.2 \pm 0.2$  and  $3.3 \pm 0.1$  for  $^{\text{peg}}\text{RhOG}$  and  $^{\text{lpeg}}\text{RhOG}$ , respectively (**Figure 3.17** and **3.18**). Control experiments with Oregon Green alone and 1:1 mixtures of Oregon Green:Rh(phen)(chrysi)( $^{\text{peg}}\text{bpy}$ ) $^{3+}$  and Oregon Green:Rh(phen)(chrysi)( $^{\text{lpeg}}\text{bpy}$ ) $^{3+}$  display no mismatch-dependent differences in fluorescence. Likewise, neither  $^{\text{peg}}\text{RhOG}$  nor  $^{\text{lpeg}}\text{RhOG}$  show any fluorescence

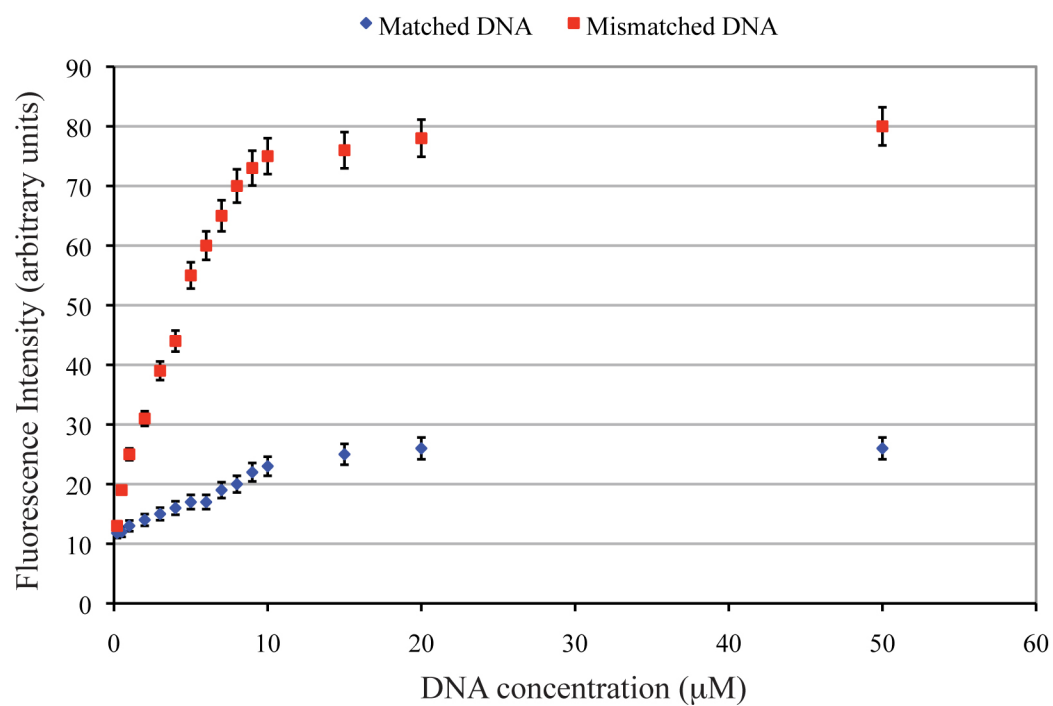


**Figure 3.17: Fluorescence of <sup>peg</sup>RhOG with matched and mismatched DNA.** At saturating DNA concentrations, <sup>peg</sup>RhOG shows a relative intensity with mismatched versus matched DNA of  $3.2 \pm 0.2$ .

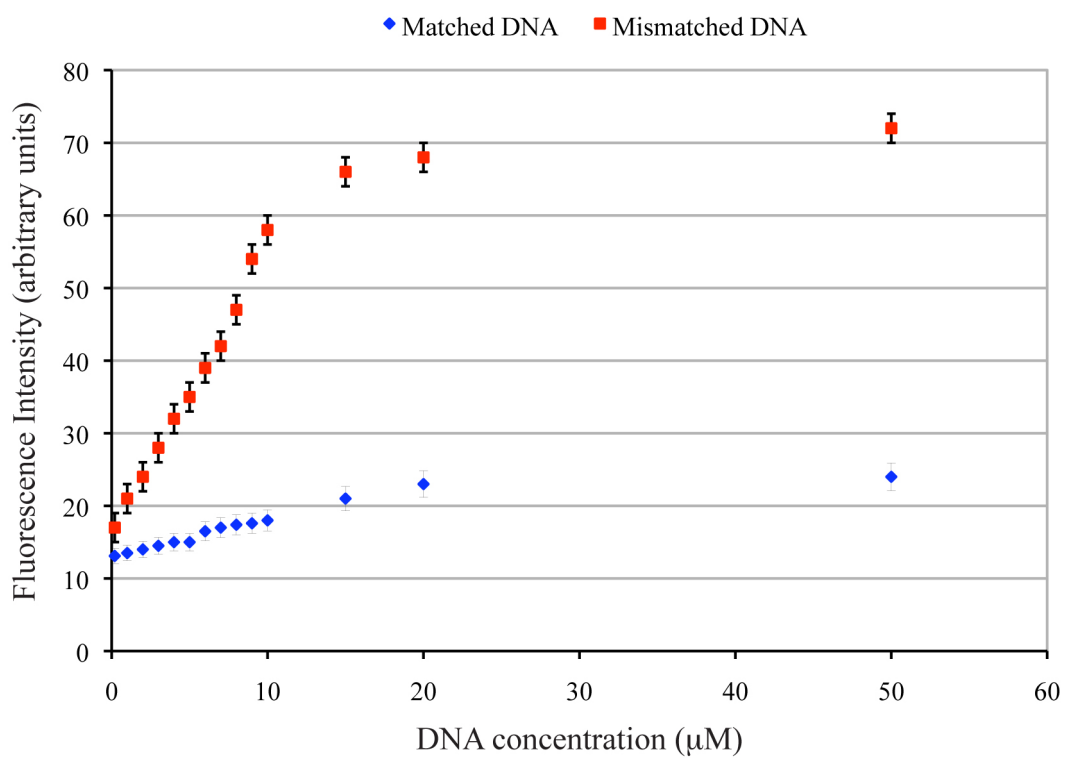


**Figure 3.18: Fluorescence of  $^{1\text{peg}}\text{RhOG}$  with matched and mismatched DNA.** At saturating DNA concentrations,  $^{1\text{peg}}\text{RhOG}$  shows a relative intensity with mismatched versus matched DNA of  $3.3 \pm 0.1$ .

enhancement with single stranded DNA. Interestingly, no DNA-dependent (mismatched or matched) changes in fluorescence anisotropy are observed for either conjugate, suggesting that the fluorophore moiety is exceedingly mobile in the DNA-bound form.

Taken together, the data for <sup>peg</sup>RhOG and <sup>lpeg</sup>RhOG represent a significant success in the optimization of the initial bifunctional conjugate system. By employing a longer, more flexible linkers, the ratios of the fluorescence intensities of the conjugates with mismatched to matched DNA increase almost threefold. However, it would be remiss not to note one important caveat: even in the presence of mismatched DNA, the conjugates are significantly quenched, with only 6% of the fluorescence intensity of an equimolar, 1:1 solution of free fluorophore and metalloinsertor and 3% compared to that of the free fluorophore alone.

### 3.3: CONCLUSIONS

This work establishes a simple yet effective strategy for the design of a bifunctional metalloinsertor-fluorophore conjugate that serves as a fluorescent probe for mismatched DNA. All four of the conjugates synthesized selectively bind and photocleave DNA, while the two with the longest and most flexible linkers show significantly enhanced fluorescence with mismatched DNA compared to matched DNA. Thus, it becomes clear that this work stands not only as a proof-of-concept for a novel mismatch-specific fluorophore but also as an instructive study on the importance of linker optimization in the design of bifunctional conjugates.

### 3.4: EXPERIMENTAL PROTOCOLS

Many of the procedural details for this investigation are included in Chapter 2 of this text. These include the following: the syntheses of Rh(phen)(chrysi)(NH<sub>3</sub>)<sub>2</sub><sup>3+</sup> (2.3.4.1–2.3.4.5), <sup>NH<sub>2</sub></sup>bpy (2.3.5.1–2.3.5.3), and <sup>peg</sup>bpy (2.3.5.4–2.3.5.6); the synthesis, purification, and radiolabeling of oligonucleotides (2.4.1–2.4.2); the Maxam-Gilbert sequencing of radiolabeled DNA (2.4.3); and the performance of recognition and binding titration experiments via PAGE (2.4.4.1–2.4.4.2). Experimental details of the fluorimetry measurements discussed herein are included above in Section 3.2.

#### 3.4.1: MATERIALS AND INSTRUMENTATION

All reagents were obtained from commercial sources and used as received without further purification. RhCl<sub>3</sub> was purchased from Pressure Chemicals. Oregon Green 514<sup>TM</sup> succinimidyl ester was purchased from Molecular Probes (Invitrogen) and stored at -20 °C. All non-aqueous solvents were purchased from Fluka and stored under argon and over molecular sieves. All water used was purified using a MilliQ water purification system. Unless otherwise noted, all reactions were performed under ambient conditions.

<sup>1</sup>H-NMR spectra were recorded on a Varian 300 MHz spectrometer at room temperature using solvent residual signal as a reference to TMS. Mass spectrometry was performed at either the Caltech mass spectrometry facility or in the Beckman Institute Protein/Peptide Micro Analytical Laboratory (PPMAL). Absorption spectra were recorded on a Beckman DU 7400 spectrophotometer. Extinction coefficients were determined using inductively coupled plasma mass spectrometry. All fluorescence measurements were taken on an ISS K2 fluorimeter (5 mm path length) equipped with a

250 W xenon lamp as an excitation source. Unless otherwise noted, an excitation wavelength of 475 nm was employed, and fluorescence experiments were performed using 1  $\mu$ M fluorophore of interest in a buffer of 20 mM NaCl, 10 mM NaPi, pH 7.1. All experiments were performed in triplicate.

Oligonucleotides were synthesized on an ABI 3400 DNA synthesizer and purified via HPLC in duplicate (DMT-off and DMT-on) before use. All reverse-phase HPLC purifications were performed on an HP1100 high-pressure liquid chromatography system equipped with diode array detector using a Varian DynaMax C18 semipreparative column (see Chapter 2, Section 2.4.1). Irradiations were performed using an Oriel Instruments solar simulator (320-440 nm). All PAGE experiments described employed denaturing 20% polyacrylamide gels (SequaGel, National Diagnostics) and were performed according to published procedures. Further, gels were developed using Molecular Dynamics phosphorimaging screens and a Molecular Dynamics Storm 820 phosphorimager and were subsequently visualized and quantified with Molecular Dynamics ImageQuant software.

### **3.4.2: SYNTHESIS OF 11-(4'-METHYL-2,2'-BIPYRIDIN-4-YL)UNDECAN-1-AMINE (<sup>EL</sup>-BPY)**

#### **3.4.2.1: ALKYLATION**

A 50 mL Schlenk flask was flame-dried and subjected to three rounds of evacuation and re-filling with Ar(g). The flask was then charged by syringe with 3.9 mL (28 mmol) diisopropylamine, and 20 mL THF (dry and under argon, Fluka) were transferred into the flask via cannula. The flask was cooled to -78 °C in a dry ice/acetone

bath, followed by the dropwise addition of 13.5 mL (27 mmol) 2 M BuLi. The resultant light yellow LDA solution was kept at  $-78\text{ }^{\circ}\text{C}$  as the reaction vessel was prepared.

A 500 mL, three-necked round-bottom flask was flame-dried, charged with 5 g (27 mmol) 4,4'-dimethyl-2,2'-bipyridine, and subjected to three rounds of evacuation and refilling with  $\text{Ar}_{(\text{g})}$ . 200 mL THF (dry and under argon, Fluka) were transferred into the flask via cannula, and the reaction mixture was cooled to  $-78\text{ }^{\circ}\text{C}$  in a dry ice/acetone bath. The LDA solution was then transferred into the 500 mL round-bottom flask via cannula, and the resultant dark brown reaction mixture was allowed to stir at  $-78\text{ }^{\circ}\text{C}$  for 1 h. After 1 h, 40 g (5 equiv.) dibromohexane were added to the reaction via syringe. The reaction mixture was immediately transferred to a dry ice bath (i.e. no acetone) and allowed to warm slowly to room temperature over the next 16 h. During this time, the reaction changed colors dramatically from brown to dark green to green to dark yellow and, finally, to light yellow.

Once at room temperature, the reaction vessel was opened to air, and  $\text{H}_2\text{O}$  (150 mL) was added to the reaction mixture to quench any remaining LDA. The pH of the mixture was adjusted to  $\sim 10$  with saturated  $\text{NaHCO}_{3(\text{aq})}$ . The basified reaction mixture was then extracted once with 50 mL  $\text{Et}_2\text{O}$  and subsequently with 50 mL increments of  $\text{CH}_2\text{Cl}_2$  until the organic layer no longer stains red when spotted on a TLC plate (silica) and dipped in an Fe(II) solution. At this point ( $\sim 250$  mL total volume organic layer), the organic layer was washed with brine, dried over  $\text{MgSO}_4$ , filtered, and concentrated *in vacuo* to yield the final product as a yellow oil.

The crude product was purified via column chromatography (SiO<sub>2</sub> pretreated with 1:10 NEt<sub>3</sub>:hexanes) with a solvent system of 1:1 EtOAc:Hexanes. The purified product, nicknamed <sup>elBr</sup>bpy, is a white solid (7.3 g).

<sup>1</sup>H-NMR (CD<sub>2</sub>Cl<sub>2</sub>): 8.53 ppm (split d, 2H); 8.28 ppm (s, 2H); 7.16 ppm (d, 2H); 3.42 ppm (t, 2H); 2.70 ppm (t, 2H); 2.44 ppm (s, 3H); 1.87 ppm (m, 2H); 1.7 ppm (m, 2H); 1.5–1.1 ppm (m, 14H).

ESI-MS (m/z): 403, 405 [M+H]<sup>+</sup>

#### 3.4.2.2: PHTHALIMIDE SUBSTITUTION

The bromide-terminated linker was converted to an amine-terminated linker by an adapted Gabriel amine synthesis. In a 250 mL round-bottom flask, <sup>elBr</sup>bpy (0.35 g) was combined with potassium phthalamide (0.240 g) in 35 mL DMF and heated to 130 °C for 12 h. After cooling to room temperature, water (100 mL) was added, and the reaction mixture was brought to ~ pH 10 with saturated NaHCO<sub>3(aq)</sub>. This solution was then extracted three times with 75 mL CH<sub>2</sub>Cl<sub>2</sub>, washed once with brine, dried over MgSO<sub>4</sub>, and evaporated to dryness to yield a white solid (515 mg, > 95%, <sup>elphth</sup>bpy) that was pure by TLC (SiO<sub>2</sub>, 1:1 EtOAc:Hex).

ESI-MS (m/z): 470 [M+H]<sup>+</sup>, 492 [M+Na]<sup>+</sup>

#### 3.4.2.3: HYDROLYSIS

In a 250 mL round-bottom flask, <sup>elphth</sup>bpy (250 mg, 0.53 mmol) was dissolved in EtOH (50 mL) by heating to 60 °C for 30 min. After 30 min, hydrazine monohydrate (0.2 mL, 4.1 mmol, 8 equiv.) was added, and the reaction mixture was stirred at 70 °C for 16

h. After cooling to room temperature, the solvent was removed *in vacuo*. The residue was taken up in 50 mL chloroform and extracted five times with 50 mL 1 M hydrochloric acid. The acid phase was then extracted twice with 50 mL CHCl<sub>3</sub> to eliminate any residual phthalimide products. The pH of the combined aqueous layers was then adjusted to ~10 with saturated NaHCO<sub>3</sub> solution, and the newly basic aqueous layer was extracted four times with 50 mL CHCl<sub>3</sub>, washed with brine, dried over MgSO<sub>4</sub>, and dried *in vacuo* to yield a white solid that was pure by NMR (100 mg, 70%, nicknamed <sup>el</sup>bpy).

<sup>1</sup>H-NMR (CD<sub>2</sub>Cl<sub>2</sub>): 8.47 ppm (m, 2H); 8.20 ppm (m, 2H); 7.10 ppm (m, 2H); 2.85 ppm (m, 2H); 2.65 ppm (m, 2H); 2.41 ppm (s, 3H); 1.6 ppm (m, 4H); 1.4–1.2 ppm (m, 18H).

ESI-MS (m/z): 340 [M+H]<sup>+</sup>, 380 [M+K]<sup>+</sup>

### 3.4.3: SYNTHESIS OF *N*-(2-(2-(2-AMINOETHOXY)ETHOXY)ETHYL)-8-(4'-METHYL-2,2'-BIPYRIDIN-4-YL)OCTANAMIDE (<sup>LPEG</sup>BPY)

The first step in the synthesis of <sup>lpeg</sup>bpy is the monoalkylation of 4,4'-dimethylbipyridine to make <sup>Br</sup>bpy. This procedure is detailed in Chapter 2 of this work under 2.3.5.1.

#### 3.4.3.1: CYANIDE SUBSTITUTION

In a 250 mL round-bottom flask, <sup>Br</sup>bpy (500 g, 1.4 mmol) was combined with potassium cyanide (200 mg, 3.125 mmol) in 100 mL DMSO and heated to 90 °C for 12 h. After cooling to room temperature, water (100 mL) was added, and the reaction mixture was brought to pH ~ 10 with saturated NaHCO<sub>3(aq)</sub>. This solution was then

extracted three times with 75 mL CH<sub>2</sub>Cl<sub>2</sub>, washed once with brine, dried over MgSO<sub>4</sub>, and evaporated to dryness to yield a white solid (300 mg, 71%, nicknamed <sup>CN</sup>bpy) that was pure by TLC (SiO<sub>2</sub>, 1:1 EtOAc:Hex).

ESI-MS (m/z): 294 [M+H]<sup>+</sup>

### 3.4.3.2: HYDROLYSIS

In a 100 mL round-bottom flask, <sup>CN</sup>bpy (300 mg, 1.2 mmol) was dissolved in a mixture of 20 mL concentrated HCl and 5 mL concentrated H<sub>2</sub>SO<sub>4</sub> and refluxed at 70 °C overnight. After 16 h, H<sub>2</sub>O (100 mL) was added to the reaction mixture, and the pH was adjusted to 4.0 with NaOH(s). The aqueous layer was extracted with CH<sub>2</sub>Cl<sub>2</sub> (4 x 50 mL). At this point (~ 200 mL total volume CH<sub>2</sub>Cl<sub>2</sub>), the organic layer was washed with brine, dried over MgSO<sub>4</sub>, filtered, and concentrated *in vacuo* to yield the carboxylic acid as a white solid (bpy'', 250 mg, 80%).

ESI-MS (m/z): 312.3 [M+H]<sup>+</sup>

### 3.4.3.3: FORMATION OF THE SUCCINIMIDYL ESTER

In a 250 mL round-bottom flask, 210 mg bpy'' (0.67 mmol), 86 mg N-hydroxysuccinimide (0.75 mmol), and 150 mg DCC (0.75 mmol) were dissolved in 100 mL CH<sub>2</sub>Cl<sub>2</sub>. The solution was stirred for 2 h at room temperature. After 2 h, a precipitate had become apparent, and the reaction was placed in the cold room overnight to facilitate precipitation. In the morning, the solution was filtered, and the filtrate was reduced *in vacuo* to reveal the pure N-succinimidyl ester product as a clear oil (250 mg, 0.6 mmol, 90%).

ESI-MS (m/z): 410 [M+H]<sup>+</sup>, 432 [M+Na]<sup>+</sup>

#### 3.4.3.4: COUPLING

In a 25 mL pear-shaped flask, 100 g of the NHS-ester were dissolved in 3 mL DMF, and a solution of 2 mL (excess) of 2,2'-(ethylenedioxy)bis(ethylamine) in 1 mL DMF was added. After two h of stirring, 0.05 mL DIEA were added to ensure deprotonation of the amines. The reaction mixture was stirred for 15 h at room temperature. After 16 h, the reaction mixture was concentrated *in vacuo*, taken up in CH<sub>2</sub>Cl<sub>2</sub>, extracted twice with a saturated NaHCO<sub>3</sub> solution, dried over MgSO<sub>4</sub>, and re-concentrated *in vacuo*. The final product (<sup>PEG</sup>bpy) was obtained pure as a clear oil.

ESI-MS (m/z): 443.2 [M+H]<sup>+</sup>

#### 3.4.4: METALLATION OF <sup>X</sup>BPY LIGANDS

In a 100-mL round-bottom flask, Rh(phen)(chrysi)(X)<sub>2</sub> (150 mg, 0.22 mmol) was combined with <sup>X</sup>bpy (150 mg, approximately 0.6 mmol) in a 50/50 mixture of ethanol and deionized water (50 mL total volume). The reaction was stirred at reflux overnight in an oil bath. The mixture was then allowed to cool, diluted with 200 mL H<sub>2</sub>O, and purified by cation exchange chromatography.

Four inches of resin pre-equilibrated with 0.05 M MgCl<sub>2</sub> were poured into a 1–1.5 inch diameter column and subsequently washed with copious (500 mL) deionized H<sub>2</sub>O. The rhodium complex was loaded onto the column simply by passing the aqueous Rh solution through the resin (the rhodium complex will ‘stick’ to the top of the column, forming a thin, dark orange band). The complex was then eluted by slowly increasing the

[MgCl<sub>2</sub>] in the eluent in 500-mL batches, starting with 0.05 M MgCl<sub>2</sub> and increasing in increments of 0.05 M until the red band of the metal complex has passed through the column. The resultant eluted solution was concentrated on a reverse-phase cartridge primed with MeOH, eluted with 1:1:0.001 H<sub>2</sub>O/MeCN/TFA (vol/vol/vol), and lyophilized to yield the product as a red-orange powder.

ESI-MS [Rh(phen)(chrysi)(<sup>NH<sub>2</sub></sup>bpy)<sup>3+</sup>]: 820 [M+H]<sup>+</sup>, 410 [M+2H]<sup>2+</sup>

ESI-MS [Rh(phen)(chrysi)(<sup>el</sup>bpy)<sup>3+</sup>]: 873 [M+H]<sup>+</sup>, 436 [M+2H]<sup>2+</sup>

ESI-MS [Rh(phen)(chrysi)(<sup>peg</sup>bpy)<sup>3+</sup>]: 923 [M+H]<sup>+</sup>, 462 [M+2H]<sup>2+</sup>

ESI-MS [Rh(phen)(chrysi)(<sup>lpeg</sup>bpy)<sup>3+</sup>]: 979 [M+H]<sup>+</sup>, 490 [M+2H]<sup>2+</sup>

#### 3.4.5: COUPLING THE METALLOINSERTOR AND FLUOROPHORE SUBUNITS

In a flame-dried, Argon-filled 10 mL Schlenk flask, Oregon Green 514 succinimidyl ester (5 mg) and Rh(phen)(chrysi)(<sup>x</sup>bpy)<sup>3+</sup> (5 mg) were dissolved in 2 mL DMF. The resultant vessel was purged with Ar<sub>(g)</sub> for 5 min and then stirred for 2 h at room temperature. After 2 h, 0.5 mL DIEA were added, and the resultant reaction mixture was allowed to stir overnight under argon. After 16 h, H<sub>2</sub>O (4 mL) was added to the reaction mixture, and the aqueous solution was loaded onto a C18 reverse-phase cartridge (Waters Sep-Pak), washed with water, and eluted with 1:1:0.001 (H<sub>2</sub>O:MeCN:TFA). The purified product was frozen and lyophilized to dryness. Each conjugate was further purified via reverse-phase high-performance liquid chromatography using an HP1100 HPLC system, a Varian DynaMax C18 semipreparative column, and an elution gradient of 85:15 to 40:60 H<sub>2</sub>O (0.1% TFA):MeCN (0.1% TFA) over 60 min.

UV-Vis (all complexes, H<sub>2</sub>O, pH 7.0):  $\lambda_{\max}$  302 nm ( $\epsilon = 54,800$ ), 313 ( $\epsilon = 44,600$ ), and 519 ( $\epsilon = 78,000$ ).

ESI-MS (RhOG): 1316 [M+H]<sup>+</sup>, 659 [M+2H]<sup>2+</sup>

ESI-MS (<sup>el</sup>RhOG): 1370 [M+H]<sup>+</sup>, 685 [M+2H]<sup>2+</sup>

ESI-MS (<sup>peg</sup>RhOG): 1417 [M+H]<sup>+</sup>, 709 [M+2H]<sup>2+</sup>

ESI-MS (<sup>lpeg</sup>RhOG): 1473 [M+H]<sup>+</sup>, 737 [M+2H]<sup>2+</sup>

### 3.5: REFERENCES

1. Kolodner, R. D. *Trends in Biochemical Science* **1995**, *20*, 397–401.
2. Hsieh, P.; Yamane, K. *Mechanisms of Ageing and Development* **2008**, *129* (7–8), 391–407.
3. Hoffmann, J. S.; Cazaux, C. *International Journal of Oncology* **1998**, *12* (2), 377–382.
4. Scott, R. J. *Onkologie* **1997**, *20* (1), 42–47.
5. Toft, N. J.; Arends, M. J. *Journal of Pathology* **1998**, *185* (2), 123–129.
6. Bocker, T.; Ruschoff, J.; Fishel, R. *Biochimica Et Biophysica Acta—Reviews on Cancer* **1999**, *1423* (3), O1–O10.
7. Wheeler, J. M. D.; Bodmer, W. F.; Mortensen, N. J. M. *Gut* **2000**, *47* (1), 148–153.
8. Jacob, S.; Praz, F. *Biochemie* **2002**, *84*, 27–47.
9. Valentini, A. M.; Armentano, R.; Pirrelli, M.; Caruso, M. L. *Cancer Treatment Reviews* **2006**, *32* (8), 607–618.
10. Muller, A.; Korabiowska, M.; Brinck, U. *In Vivo* **2003**, *17* (1), 55–59.

11. Pors, K.; Patterson, L. H. *Current Topics in Medicinal Chemistry* **2005**, *5* (12), 1133–1149.
12. Fink, D.; Aebi, S.; Howell, S. B. *Clinical Cancer Research* **1998**, *4* (1), 1–6.
13. Jackson, B. A.; Barton, J. K. *Journal of the American Chemical Society* **1997**, *119* (52), 12986–12987.
14. Jackson, B. A.; Alekseyev, V. Y.; Barton, J. K. *Biochemistry* **1999**, *38* (15), 4655–4662.
15. Zeglis, B. M.; Barton, J. K. *Nature Protocols* **2007**, *2* (2), 357–371.
16. Zeglis, B. M.; Pierre, V. C.; Barton, J. K. *Chemical Communications* **2007**, 4565–4579.
17. Baumstark, D.; Wagenknecht, H. A. *Angewandte Chemie–International Edition* **2008**, *47* (14), 2612–2614.
18. Cho, M.; Chung, S.; Heo, S. D.; Ku, J.; Ban, C. *Biosensors & Bioelectronics* **2007**, *22* (7), 1376–1381.
19. Takei, F.; Suda, H.; Hagihara, M.; Zhang, J. H.; Kobori, A.; Nakatani, K. *Chemistry—a European Journal* **2007**, *13* (16), 4452–4457.
20. Nesterova, I. V.; Erdem, S. S.; Pakhomov, S.; Hammer, R. P.; Soper, S. A. *Journal of the American Chemical Society* **2009**, *131* (7), 2432–+.
21. Ruba, E.; Hart, J. R.; Barton, J. K. *Inorganic Chemistry* **2004**, *43* (15), 4570–4578.
22. Petitjean, A.; Barton, J. K. *Journal of the American Chemical Society* **2004**, *126* (45), 14728–14729.
23. Schatzschneider, U.; Barton, J. K. *Journal of the American Chemical Society* **2004**, *126* (28), 8630–8631.

24. Lim, M. H.; Lau, I. H.; Barton, J. K. *Inorganic Chemistry* **2007**, *46*, 9528–9530.
25. Jackson, B. A.; Barton, J. K. *Biochemistry* **2000**, *39* (20), 6176–6182.
26. Gabriel, S. *Chemische Berichte* **1887**, *20*, 2224–.
27. Gibson, M. S.; Bradshaw, R. W. *Angewandte Chemie–International Edition* **1968**, *7* (12), 919–925.
28. Della Ciana, L.; Hamachi, I.; Meyer, T. J. *Journal of Organic Chemistry* **1989**, *54* (7), 1731–1735.